

This article was downloaded by:[Bochkarev, N.]
On: 13 December 2007
Access Details: [subscription number 746126554]
Publisher: Taylor & Francis
Informa Ltd Registered in England and Wales Registered Number: 1072954
Registered office: Mortimer House, 37-41 Mortimer Street, London W1T 3JH, UK



Astronomical & Astrophysical Transactions

The Journal of the Eurasian Astronomical Society

Publication details, including instructions for authors and subscription information:
<http://www.informaworld.com/smpp/title~content=t713453505>

Gas dynamic investigation of rotating gas accretion

G. S. Bisnovatyi-kogan^a, N. V. Pogorelov^b

^a Space Research Institute, Russian Academy of Sciences, Moscow, Russia

^b Institute for Problems in Mechanics, Russian Academy of Sciences, Moscow, Russia

Online Publication Date: 01 January 1997

To cite this Article: Bisnovatyi-kogan, G. S. and Pogorelov, N. V. (1997) 'Gas dynamic investigation of rotating gas accretion', *Astronomical & Astrophysical Transactions*, 12:4, 263 - 280

To link to this article: DOI: 10.1080/10556799708232082

URL: <http://dx.doi.org/10.1080/10556799708232082>

PLEASE SCROLL DOWN FOR ARTICLE

Full terms and conditions of use: <http://www.informaworld.com/terms-and-conditions-of-access.pdf>

This article may be used for research, teaching and private study purposes. Any substantial or systematic reproduction, re-distribution, re-selling, loan or sub-licensing, systematic supply or distribution in any form to anyone is expressly forbidden.

The publisher does not give any warranty express or implied or make any representation that the contents will be complete or accurate or up to date. The accuracy of any instructions, formulae and drug doses should be independently verified with primary sources. The publisher shall not be liable for any loss, actions, claims, proceedings, demand or costs or damages whatsoever or howsoever caused arising directly or indirectly in connection with or arising out of the use of this material.

GAS DYNAMIC INVESTIGATION OF ROTATING GAS ACCRETION

G. S. BISNOVATYI-KOGAN¹ and N. V. POGORELOV²

¹*Space Research Institute, Russian Academy of Sciences, 84/32 Profsoyuznaya St,
117810 Moscow, Russia*

²*Institute for Problems in Mechanics, Russian Academy of Sciences,
101 Vernadskii Ave., Moscow 117526, Russia*

(Received November 15, 1995)

Gas dynamic features of slowly rotating axially symmetric gas accretion on to a gravitating centre are investigated. The process of flow restructuring is studied as the angular velocity of accreting matter approaches the Keplerian angular velocity. For spherically symmetric accretion the conditions are found of the existence of a steady-state state supersonic solution for various external boundary conditions. A numerical study is performed on the basis of the Lax–Friedrichs-type second-order numerical scheme with an implicit approximation of the term in the Euler equations.

KEY WORDS X-ray pulsars, accretion, gas dynamics, numerical simulation

1 INTRODUCTION

Accretion on to neutron stars and black holes produces the main energy supply in galactic X-ray sources. X-ray sources with high-mass companions include long-period pulsars whose origin is yet to be explained (Nagase, 1989; Lipunov, 1992). Owing to a high-speed stellar wind, the angular momentum of falling matter is often insufficient for accretion disk formation at the level of the Alfvénic radius, where the magnetic pressure of the neutron star is balanced by the dynamic pressure of the falling gas. The angular momentum gained, in this case, by the neutron star from the falling gas has been shown (Bisnovaty-Kogan, 1991) to be such that the equilibrium rotational period of the X-ray pulsar might be long. It is rather difficult to estimate the equilibrium rotational period because the formation of outflowing streams which carry away the angular momentum is possible (Illarionov and Kompaneetz, 1990; Lovelace *et al.*, 1995). The accretion picture is three-dimensional, and its numerical simulation is very complicated. It has been performed only for the case of accretion on to a gravitating centre, showing the presence of Rayleigh–Taylor instabilities (Matsuda *et al.*, 1989). The nature of these instabilities is unclear, and a numerical origin cannot be excluded (Steinolfson *et al.*, 1994).

To investigate the formation of long-period pulsars, a model is necessary for accretion on to a magnetized neutron star from the stellar wind in a binary. To reduce a three-dimensional problem to two dimensions, we can consider either conical accretion of non-rotating gas or accretion of slowly rotating gas on to a stationary star. In the first case (Koide *et al.*, 1991), the average angular momentum acquired by the neutron star is zero due to the flow symmetry, so it cannot be applied to long-period X-ray pulsars.

Here we used the second approach. Our aim is to consider accretion on to a magnetized star with the Alfvénic radius $R_A \gg R_*$ (star radius) taking into account an interaction between the gas and the magnetosphere, and possible outflow formation. As a first step, we consider accretion with full penetration of the gas through the magnetosphere substituted by the inner boundary with the radius R_* and neglect magnetogasdynamic effects.

Beskin and Pidoprygora (1995) presented an approximate solution for the accretion of a non-rotating gas on to a slowly rotating black hole within the framework of general relativity. In this work we consider the accretion of a rotating gas in the Newton approximation up to rotation velocities close to the Keplerian velocity.

Three different modes are usually considered to be constituent parts of astrophysical accretion and have been investigated fairly well (Bisnovatyi-Kogan, 1989; Lipunov, 1992).

- (1) Spherically symmetric accretion occurs if the star velocity v_∞ is much smaller than the speed of sound a_∞ in accreting matter, and the angular momentum is negligible.
- (2) Cylindrical accretion occurs if $v_\infty \geq a_\infty$, with the angular momentum vanishing.
- (3) Accretion disk is formed if the total angular momentum of the matter is sufficient for its formation.

Real accretion is, in fact, a combination of the above-mentioned modes.

From the gas-dynamic viewpoint, it is of interest to investigate the process of transition from regime 1 to regime 3 for $v_\infty \ll a_\infty$ as the rotational velocity of the accreting matter approaches the Keplerian velocity. We consider the polytropic flow of a perfect gas with polytropic index $\gamma = 1.4$. Calculations are performed using the second-order space high-resolution Lax–Friedrichs-type numerical scheme proposed by one of the authors (Barmin and Pogorelov, 1995). A detailed description of the scheme is given by Barmin *et al.* (1996). A three-dimensional Bondi–Hoyle accretion has been investigated recently for an accretor (star) radius varying from 10 to 0.02 Bondi radii, so that both subsonic and supersonic regimes of the accretion can be realized (Ruffert, 1994). In our study we are mainly interested in a qualitative tracing of the flow restructuring as its angular velocity increases. For this reason the Euler equations are solved, and the external flow is supposed to be supersonic. On the other hand, the star size is assumed to be sufficiently small; the inner, also supersonic, is fixed at finite distance from the gravitational centre. The effects of

the boundary conditions on the existence and properties of a stationary supersonic accretion for the chosen computational region are investigated.

2 SPHERICALLY SYMMETRIC SUPERSONIC ACCRETION

Let us consider accretion gas flow between two spheres with the inner and outer radii equal to R_* and R_0 , respectively. If the flow at a distance R_0 is assumed to be supersonic, then all flow parameters should be fixed at this boundary. The question is what parameter values can be imposed at a given distance for the existence of a stationary solution. If the flow is shockless and polytropic, the following three conservation equations must be satisfied:

$$4\pi R^2 \rho U = \dot{M}, \tag{1}$$

$$\frac{p}{\rho^\gamma} = K, \tag{2}$$

$$\frac{U^2}{2} + \frac{\gamma}{\gamma-1} \frac{p}{\rho} - \frac{GM}{R} = h_{t0}. \tag{3}$$

Here ρ , p , U are, density, pressure and radial velocity, respectively, R is a current distance from the gravitating centre, M is the star's mass. The values of the accretion rate \dot{M} , the constant K , and the Bernoulli constant h_{t0} are fixed at $R = R_0$. Introducing dimensionless variables with the units of velocity, pressure, density, and length equal to U_0 , $\rho_0 U_0^2$, ρ_0 , and R_* , respectively, and designating $M_0 = U_0/a_0$, $a_0 = (\gamma p_0/\rho_0)^{1/2}$ and $S = GM/U_0^2 R_*$, we can rewrite system (1)–(3) in a dimensionless form using the same notations for dimensionless values of U , R , p , ρ , and $a = (\gamma p/\rho)^{1/2}$ (indices 0 and * correspond to the outer and inner boundaries, respectively):

$$\frac{U^2}{2} + \frac{a^2}{\gamma-1} - \frac{S}{R} = \frac{1}{2} + \frac{1}{(\gamma-1)M_0^2} - \frac{S}{R_0}, \tag{4}$$

$$\rho U = \frac{R_0^2}{R^2}, \tag{5}$$

$$\frac{p}{\rho^\gamma} = \frac{1}{\gamma M_0^2}. \tag{6}$$

Being subsonic at infinity and supersonic at $R = R_0$, the flow becomes sonic $U = U_B = a_B$ at some point $R = R_B \geq R_*$, where (Bisnovatyi-Kogan, 1989)

$$U_B = a_B = \frac{1}{2} \frac{S}{R_B}. \tag{7}$$

At the sonic point equations (4)–(7) reduce to

$$\frac{5-3\gamma}{4(\gamma-1)} \frac{S}{R_B} = h_{t0}. \tag{8}$$

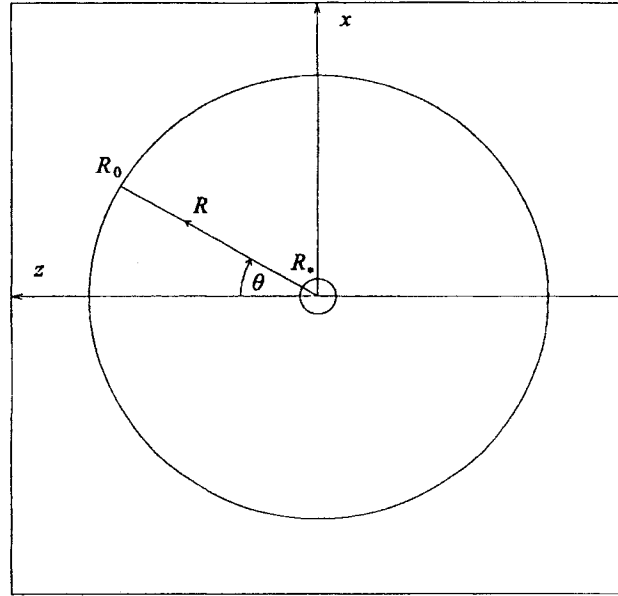


Figure 1 The computational region.

If $R_B \geq R_0$ and the flow comes from infinity, the value h_{t0} must satisfy the inequality

$$0 < h_{t0} < \frac{5 - 3\gamma}{4(\gamma - 1)R_0} S. \quad (9)$$

3 ACCRETION WITH ROTATION

In this section we consider the process of the axially symmetric rotating flow accretion on to a gravitating object. The analysis is performed on the basis of a numerical solution to the Euler gas-dynamic equations. The gas is assumed to be perfect with the following caloric equation of state: $\varepsilon = p/(\gamma - 1)\rho$, where ε is the internal energy per unit mass and $\gamma = 1.4$ is the polytropic index. The system of governing equations in the Cartesian coordinate system, shown in Figure 1, reads:

$$\frac{\partial \mathbf{U}}{\partial t} + \frac{\partial \mathbf{E}}{\partial x} + \frac{\partial \mathbf{G}}{\partial z} + \mathbf{H} = 0, \quad (10)$$

where

$$\mathbf{U} = \begin{bmatrix} \rho \\ \rho u \\ \rho v \\ \rho w \\ e \end{bmatrix}, \quad \mathbf{E} = \begin{bmatrix} \rho u \\ \rho u^2 + p \\ \rho uv \\ \rho uw \\ (e + p)u \end{bmatrix}, \quad \mathbf{G} = \begin{bmatrix} \rho w \\ \rho uw \\ \rho vw \\ \rho w^2 + p \\ (e + p)w \end{bmatrix},$$

$$\mathbf{H} = \frac{\rho}{x} \begin{bmatrix} u \\ (u^2 - v^2) + GMx \frac{\sin \theta}{R^2} \\ 2uv \\ uw + GMx \frac{\cos \theta}{R^2} \\ \frac{(e+p)u}{\rho} + GMx \frac{u \sin \theta + w \cos \theta}{R^2} \end{bmatrix}$$

Here $e = p/(\gamma - 1) + \rho(u^2 + v^2 + w^2)/2$ is the total energy per unit volume. As far as the gravitational field is considered spherically symmetric, the polar computational domain (R, θ) is chosen with the inner and outer radii equal to R_* and R_0 , respectively (see Figure 1). On normalizing the quantities of density, pressure, and velocity by ρ_0 , $\omega_* R_*$, $\rho_0 \omega_*^2 R_*^2$, where ρ_0 is the density at $R = R_0$ and ω_* is the gas angular velocity at $R = R_*$ at the equator for a constant angular momentum distribution, the source term can be rewritten in the dimensionless form as

$$\mathbf{H} = \frac{\rho}{x} \begin{bmatrix} u \\ (u^2 - v^2) + Sx \frac{\sin \theta}{R^2} \\ 2uv \\ uw + Sx \frac{\cos \theta}{R^2} \\ \frac{(e+p)u}{\rho} + Sx \frac{u \sin \theta + w \cos \theta}{R^2} \end{bmatrix} \quad (11)$$

Here $S = GM/\omega_*^2 R_*^3$. The form of the other vector components in equation (10) remains unchanged.

From now on we consider only dimensionless parameters.

The following procedure is used to construct the initial and boundary conditions.

- (1) Introducing a dimensionless parameter $\alpha = U_0/U_{K*}$, where U_0 is the radial velocity on the outer boundary and $U_{K*} = (GM/R_*)^{1/2}$ is the Keplerian velocity on the inner boundary, we fix the values on the outer boundary as if the flow were spherically symmetric:

$$\rho_0 = 1; \quad U_0 = \alpha S^{1/2}; \quad p_0 = \alpha^2 S/\gamma M_0^2; \quad W_0 = 0,$$

where W_0 is the θ -component of the velocity and $M_0 = U_0/a_0$.

The corresponding parameter values inside the computational region are adopted equal to those at the boundary.

We can find the dimensionless values of entropy and total enthalpy as follows:

$$\frac{p_0}{\rho_0^\gamma} = K; \quad h_{t0} = S \left\{ \alpha^2 \left(\frac{1}{(\gamma - 1)M_0^2 + \frac{1}{2}} \right) - \frac{1}{R_0} \right\}.$$

- (2) the following initial distribution of the angular velocity is assumed:

$$\begin{cases} \omega = \frac{1}{x^2} = \frac{1}{R^2 \sin \theta} & \text{if } R > 20 \text{ (constant angular momentum)} \\ \omega = 0.0025 & \text{if } R \leq 20 \text{ (constant angular velocity)} \end{cases}$$

The y -component v (normal to the plane of Figure 1) of the velocity \mathbf{v} is then $v = \omega x$.

- (3) The values of ρ and p in the whole computational region are modified. Assuming $U(R, \theta) = U_0$ and $W(R, \theta) = 0$, we find new pressure and density values from the formulae

$$\frac{\gamma}{\gamma - 1} \frac{p}{\rho} + \frac{U^2}{2} + \frac{v^2}{2} - \frac{S}{R} = h_{i0}; \quad \frac{p}{\rho^\gamma} = K.$$

After this all values on the external boundary are fixed because it is supersonic. No boundary conditions are necessary on the inner circle, since the flow through it is supersonic.

4 NUMERICAL SCHEME

A point clustering towards the internal boundary circle is performed to obtain a sufficiently fine flow resolution in the vicinity of the gravitating centre. The following formula is used:

$$R = R_* + (R_0 - R_*) \frac{e^{\beta\xi} - 1}{e^\beta - 1},$$

with the clustering parameter β .

If we introduce a polar mesh

$$\begin{aligned} \xi_l &= (l - 1)\Delta\xi, \quad l = 1, 2, \dots, L; \quad \theta_n = (n - 2.5)\Delta\theta, \quad n = 1, 2, \dots, N; \\ R_l &= R(\xi_l), \quad \Delta\xi = 1/(L - 1), \quad \Delta\theta = \pi/(2N - 8) \end{aligned}$$

with the centre in the accretor position, then for each cell system (1) in a finite-volume formulation takes the form

$$\begin{aligned} R_l \Delta R_l \Delta \theta \frac{\partial \mathbf{U}_{l,n}^k}{\partial t} + (R_{l+1/2} \bar{\mathbf{E}}_{l+1/2,n}^k + R_{l-1/2} \bar{\mathbf{E}}_{l-1/2,n}^k) \Delta \theta \\ + (\bar{\mathbf{E}}_{l,n+1/2}^k + \bar{\mathbf{E}}_{l,n-1/2}^k) \Delta R_l + R_l \Delta R_l \Delta \theta \mathbf{H}_{l,n}^{k+1} = 0. \end{aligned} \quad (12)$$

Here $\Delta R_l = R_{l+1/2} - R_{l-1/2}$ and $\bar{\mathbf{E}}$ is the flux normal to the boundary defined as:

$$\bar{\mathbf{E}} = n_1 \mathbf{E} + n_2 \mathbf{G},$$

where $\mathbf{n} = (n_1, n_2)$ is a unit outward vector normal to the cell surface.

The assumption is made of a piecewise parabolic distribution of the primitive gas-dynamic parameters \mathbf{q} inside the cells to specify values on their boundaries, and slope delimiters are used to obtain the non-oscillatory property.

The averaged slope inside the cell in the radial direction is determined as (Sawada *et al.*, 1989)

$$\Delta q_l = [(2\Delta R_{l-1} + \Delta R_l)\mu + (2\Delta R_{l+1} + \Delta R_l)\nu] \Delta R_l / \chi,$$

where

$$\chi = \Delta R_{l+1} + \Delta R_l + \Delta R_{l-1}, \quad \mu = \frac{\delta q_{l+1/2}}{\Delta R_{l+1} + \Delta R_l}, \quad \nu = \frac{\delta q_{l-1/2}}{\Delta R_l + \Delta R_{l-1}}.$$

The left and right boundary values are then estimated as

$$q_{l+1/2}^L = q_l + \frac{1}{2} \tilde{\Delta} q_l, \quad q_{l-1/2}^R = q_l - \frac{1}{2} \tilde{\Delta} q_l,$$

$$\tilde{\Delta} q_l = \text{minmod}(\Delta q_l, 2\mu \Delta R_l, 2\nu \Delta R_l).$$

Here

$$\text{minmod}(a, b, c) = \begin{cases} \text{sign}(a) \min(|a|, |b|, |c|) & \text{if } bc > 0 \\ 0 & \text{otherwise.} \end{cases}$$

Found the values of \mathbf{q}^L and \mathbf{q}^R on both sides of the cell boundary, the appropriate fluxes $\bar{\mathbf{E}}$ are calculated using the modified Lax–Friedrichs formula (Barmin and Pogorelov, 1995):

$$\bar{\mathbf{E}}(\mathbf{U}^R, \mathbf{U}^L) = \frac{1}{2} [\bar{\mathbf{E}}(\mathbf{U}^L) + \bar{\mathbf{E}}(\mathbf{U}^R) - \hat{\mathbf{R}}(\mathbf{U}^R - \mathbf{U}^L)],$$

where the matrix $\hat{\mathbf{R}}$ is a positive diagonal matrix with the entries equal to the spectral radius (the maximum of eigenvalue magnitudes) of

$$\frac{\partial \bar{\mathbf{E}}}{\partial \mathbf{U}}$$

on its diagonal. This scheme is a considerable simplification of the numerical algorithm as compared with the methods based on a precise characteristic splitting of the Jacobian matrices, while preserving the non-oscillatory property. Within an accuracy of the second order, it is less dissipative than the original Lax–Friedrichs scheme. Similarly, the fluxes through another pair of cell surfaces are obtained.

As seen from equation (12) the source term is approximated implicitly to provide better stability of the numerical scheme. A proper linearization of this term performed to realize the numerical procedure of obtaining the time-converging steady-state solution:

$$\mathbf{H}^{k+1} = \mathbf{H}^k + \frac{\partial \mathbf{H}^k}{\partial \mathbf{U}^k} (\mathbf{U}^{k+1} - \mathbf{U}^k).$$

The promotion of the solution in time is performed to an accuracy of the first order using the formula:

$$\begin{aligned} (I + \frac{\partial \mathbf{H}^k}{\partial \mathbf{U}^k})(\mathbf{U}_{i,n}^{k+1} - \mathbf{U}_{i,n}^k) &= -\Delta t (R_{l+1/2} \bar{\mathbf{E}}_{i+1/2,n}^k / R_l + R_{l-1/2} \bar{\mathbf{E}}_{i-1/2,n}^k / R_l) \\ &\quad / \Delta R_l + (\bar{\mathbf{E}}_{i,n+1/2}^k + \bar{\mathbf{E}}_{i,n-1/2}^k) / R_l \Delta \theta + \mathbf{H}_{i,n}^k. \end{aligned}$$

for $t = k\Delta t$, $k = 0, 1, \dots$, and Δt defined by the CFL condition (I is the identity matrix).

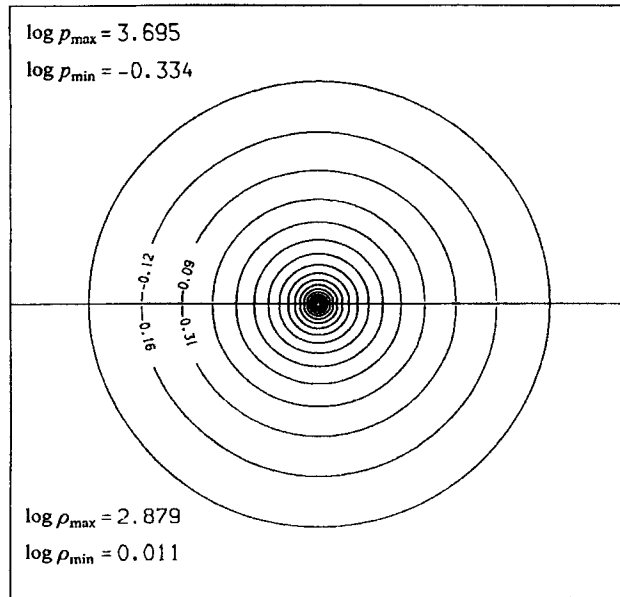


Figure 2 Logarithm pressure and density isolines. Full computational region, $S = 250$.

5 ANALYSIS OF NUMERICAL RESULTS

All the results presented in this section have been obtained in the ring region with the dimensionless inner and outer circle radii being $R_* = 1$ and $R_0 = 100$, respectively, with 56 cells in the angular direction and 104 cells in the radial direction, and with the clustering parameter $\beta = 4$. The calculations were performed until their full time-convergence had occurred in a quarter of the ring, with the appropriate reflection conditions applied in the planes of the flow symmetry.

The method presenting the results obtained is the following. In Figures 2–18 the isolines of different gas-dynamic parameters and the streamlines of the flow are presented in the lower and upper parts of the figure divided by the rotational axis. Figures 2 and 3, 7–9, and 13–15 correspond to the whole computational region. In these figures 18 isolines are presented with a constant step between the maximum and minimum values of the functions indicated in the corners, that is, the isoline value for any function f can be found from the formula $f_i = f_{\min} + i \times (f_{\max} - f_{\min})/19$. In the regions with no captions in the corner, streamlines are shown. Figures 4–6, 10–12, and 16–18 present the magnified central part (50 computational zones) of the corresponding figures related to the whole computational region.

The following dimensionless parameters are chosen primarily to study the accretion flow behaviour for the case of slow rotation (this choice is consistent with considerations from Section 2):

$$\alpha = 0.1; \quad \gamma = 1.4; \quad M_0 = 1; \quad S = 250.$$

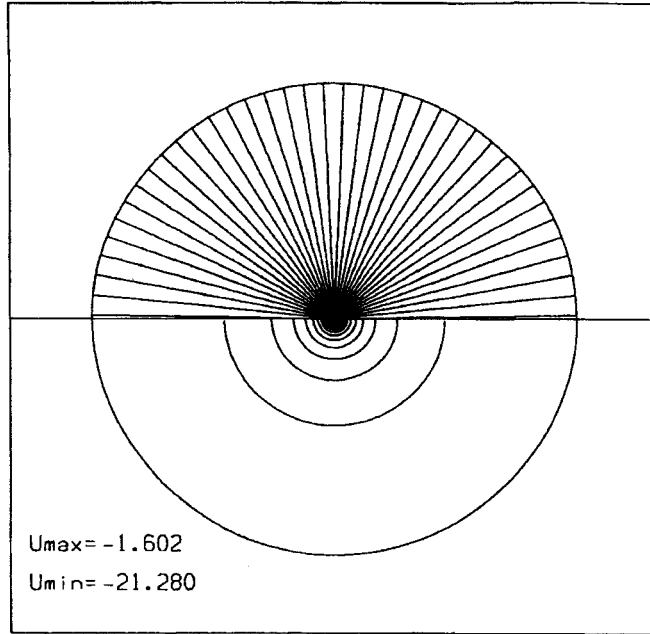


Figure 3 Streamlines and U isolines. Full computational region, $S = 250$.

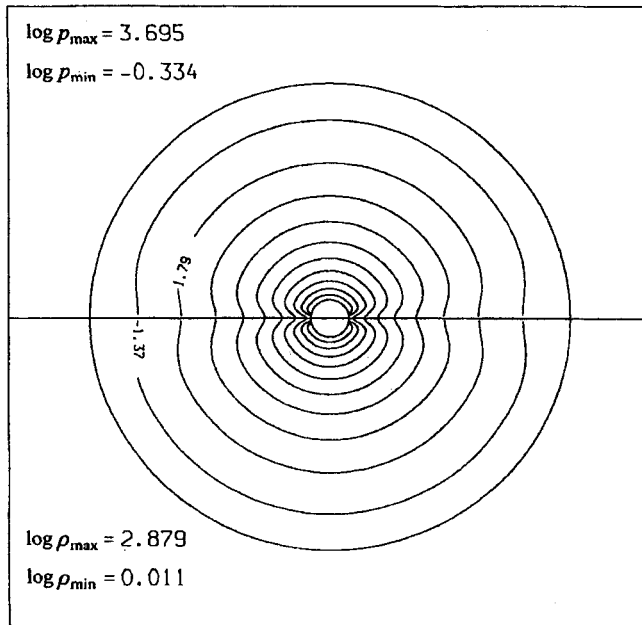


Figure 4 Logarithm pressure and density isolines. Inner subregion, $S = 250$.

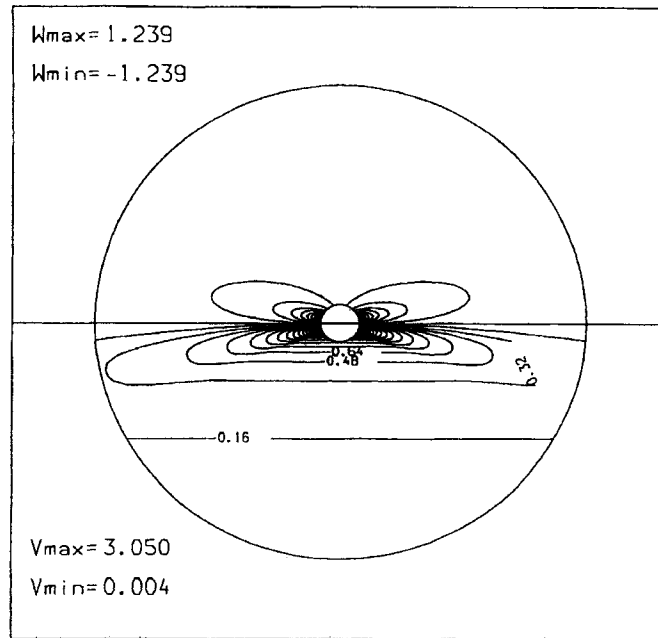


Figure 5 Isolines of v and W . Inner subregion, $S = 250$.

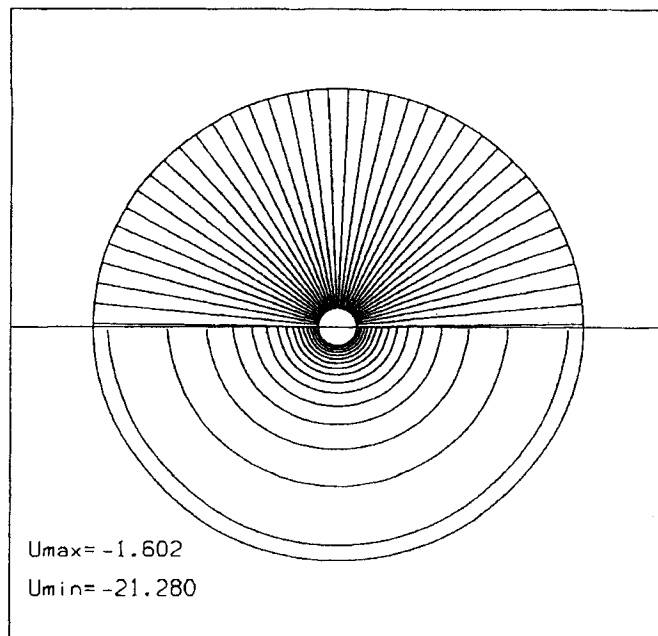


Figure 6 Streamlines and U isolines. Inner subregion, $S = 250$.

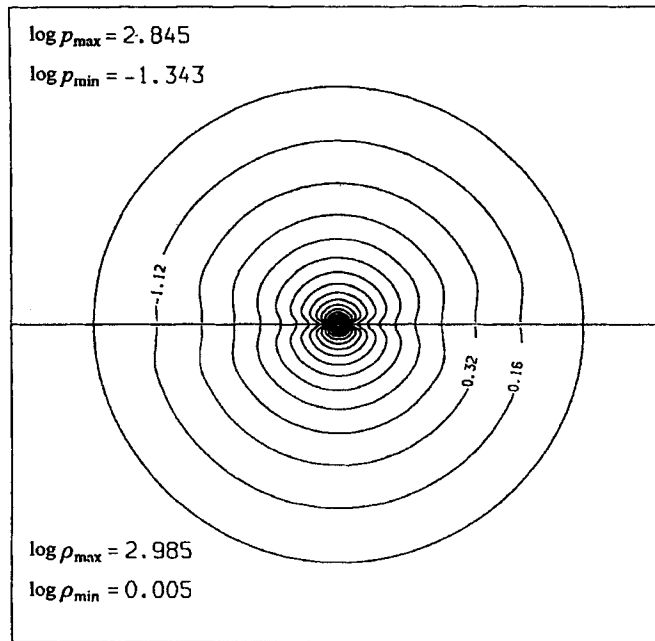


Figure 7 Logarithm pressure and density isolines. Full computational region, $S = 25$.

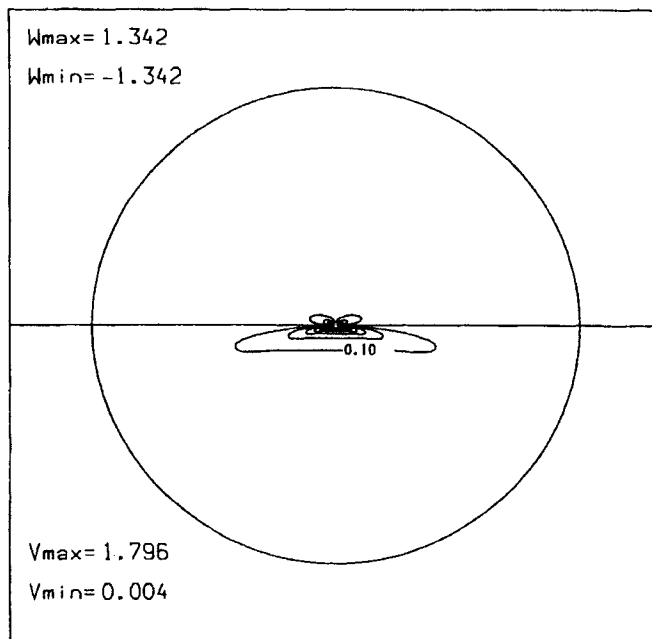


Figure 8 Isolines of v and W . Full computational region, $S = 25$.

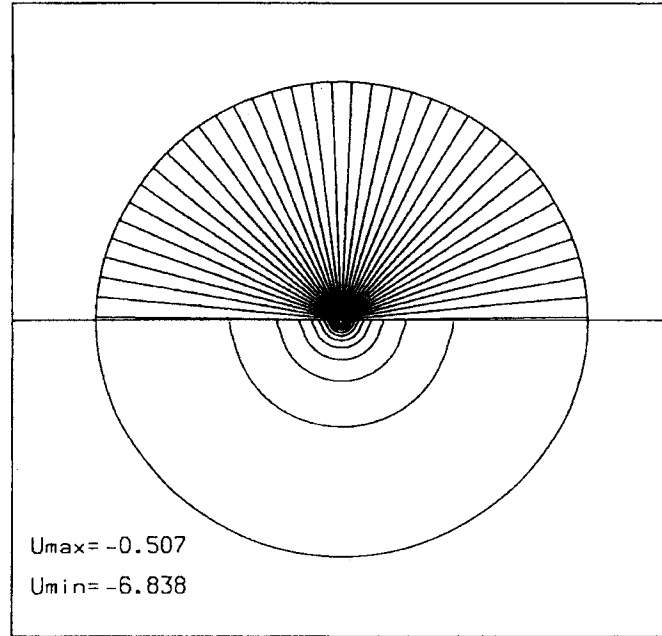


Figure 9 Streamlines and U isolines. Full computational region, $S = 25$.

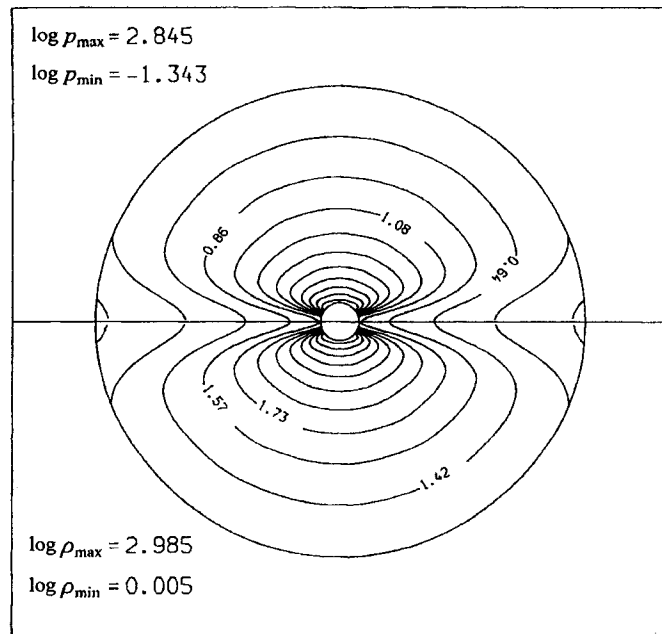


Figure 10 Logarithm pressure and density isolines. Inner subregion, $S = 25$.

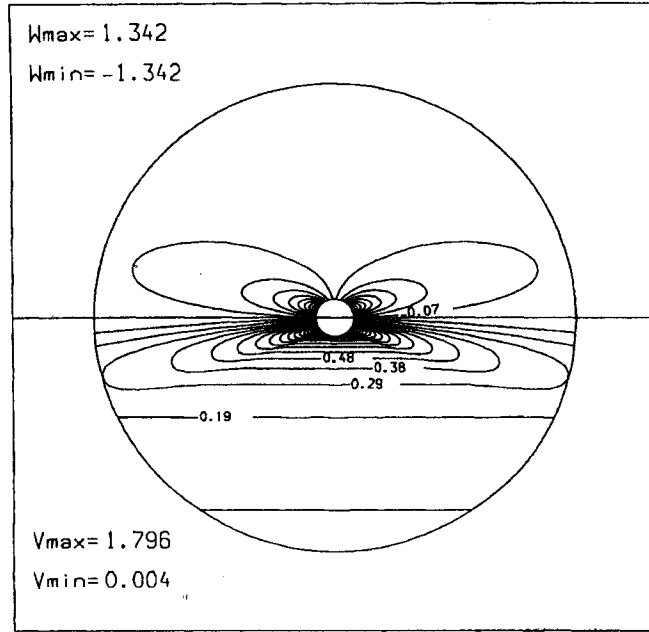


Figure 11 Isolines of v and W . Inner subregion, $S = 25$.

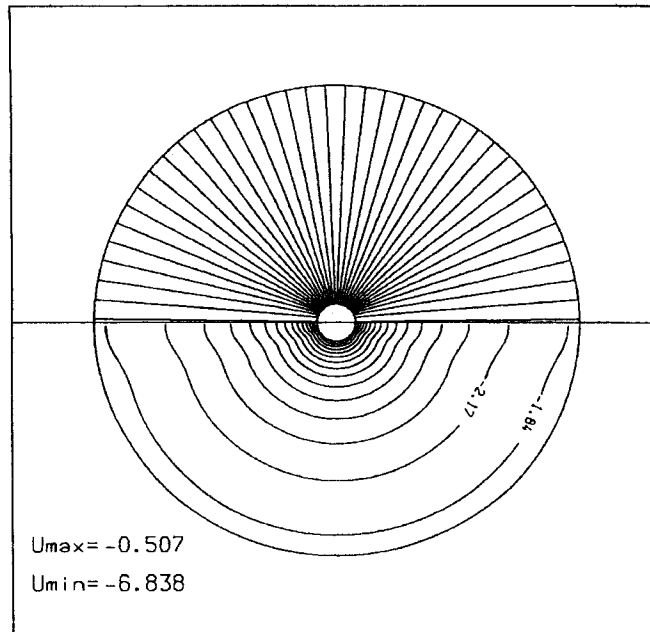


Figure 12 Streamlines and U isolines. Inner subregion, $S = 25$.

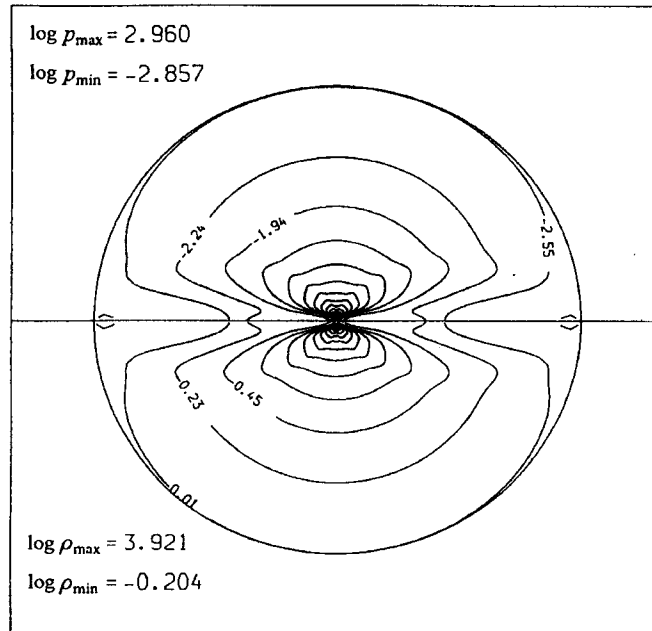


Figure 13 Logarithm pressure and density isolines. Full computational region, $S = 1.5$.

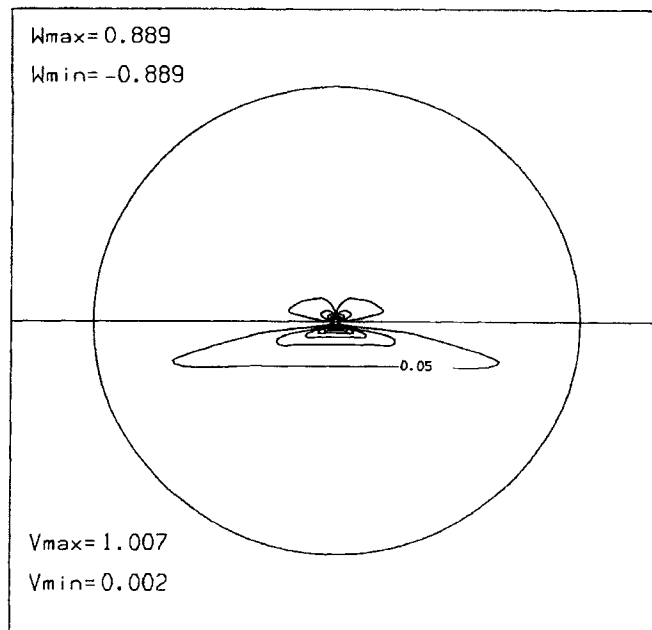


Figure 14 Isolines of v and W . Full computational region, $S = 1.5$.

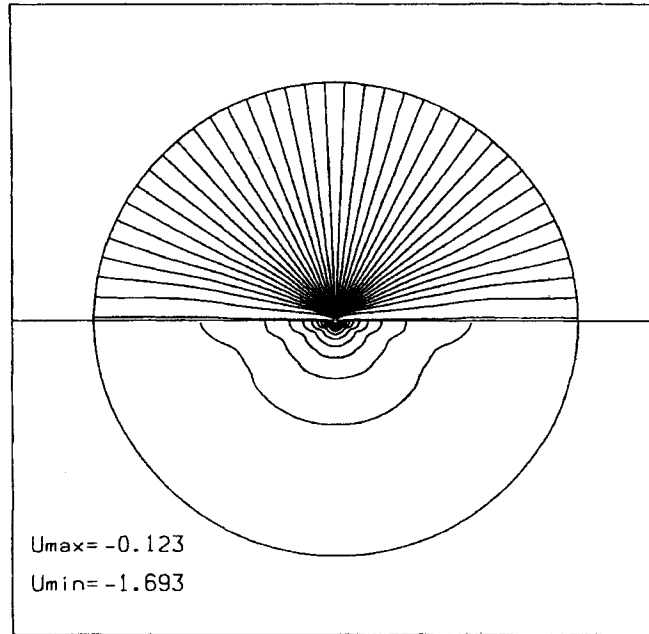


Figure 15 Streamlines and U isolines. Full computational region, $S = 1.5$.

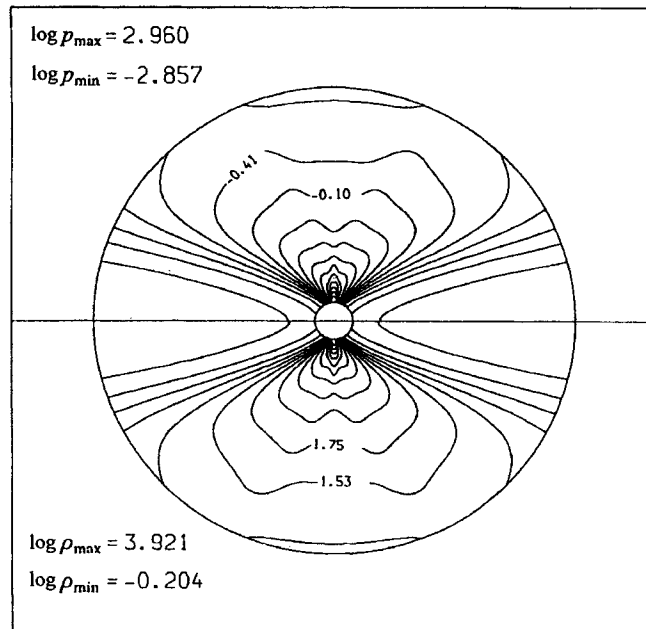


Figure 16 Logarithm pressure and density isolines. Inner subregion, $S = 1.5$.

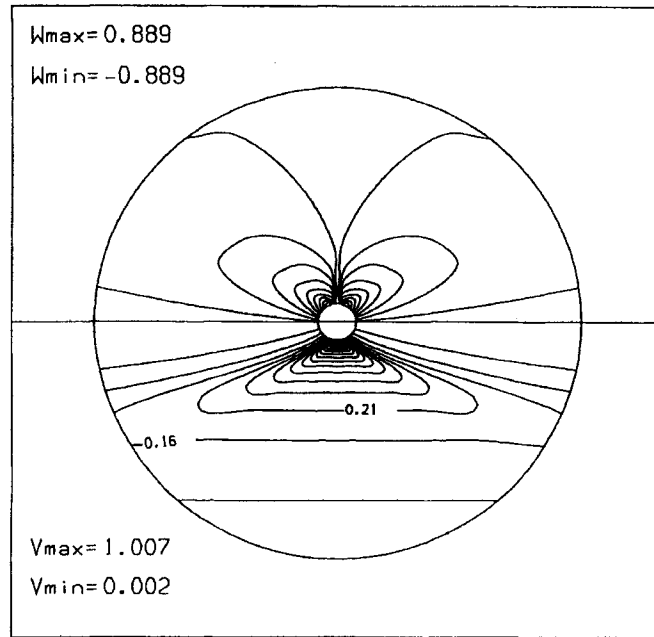


Figure 17 Isolines of v and W . Inner subregion, $S = 1.5$.

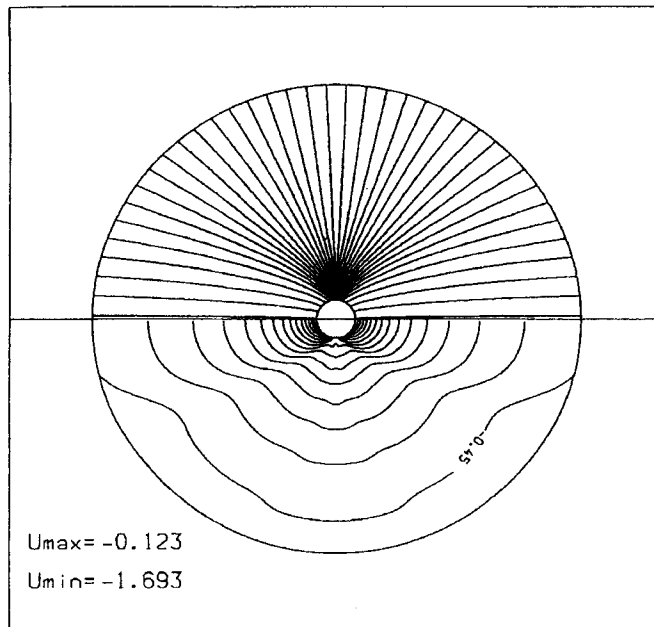


Figure 18 Streamlines and U isolines. Inner subregion, $S = 1.5$.

The steady-state results for this case are presented in Figures 2–6 (the axis of rotation is aligned with the z -axis (see Figure 1). In Figure 2, the isolines of the pressure and the density decimal logarithm are presented above and below the rotational axis, respectively, in the whole computational region. The isolines of the velocity components v and W (θ -direction) are not shown in the full computational region since their main variation is located in the vicinity of the inner boundary. The isolines of the velocity component U (radial direction) and the streamlines are given in Figure 3.

In Figures 4–6 the same lines are shown in the magnified subregion close to the accreting centre (50 computational zones). It is clearly seen in these figures that for long distances from the accreting centre and well away from the rotational axis a slow rotation does not affect the flow significantly and it is, in fact, a superposition of a spherically symmetric accretion and an axially symmetric constant angular momentum rotation. Closer to the z -axis and to the accreting centre, however, the pressure and the density are greater at the equator than near the poles. Deviation from a purely constant angular momentum rotation appears only in the vicinity of the rotational axis and near the accreting object. The streamlines and the radial velocity U isolines behave just as they do in the spherically symmetric case.

Similar pictures of the flow are presented for $S = 25$, with the rest of dimensionless parameters unchanged, in Figures 7–12. The effect of rotation in this case is quite definite in the whole region surrounding the rotational axis. The gas displacement from the poles is much more pronounced as compared with the case of $S = 250$ even at large distances from the accretion centre (see Figure 7). The streamlines defect from the poles to the region of the equator (Figure 12), and the size of the domain with substantial values of W is larger (Figures 8 and 11).

The picture of the flow for the rotational velocity close to the Keplerian velocity ($S = 1.5$) is shown in Figures 13–18. Almost all gas is removed in this case from the pole regions. The density near the equator is $\sim 10^4$ times greater than that near the poles and almost all accreting matter is involved in the motion towards $\theta = \pi/2$. The structure of the flow is very close to the picture of accretion disk formation, Figure 18 showing the streamline distribution. The regions with a dense distribution of pressure and density isolines (Figure 16) represent the oblique transverse shock where the supersonic flow of the gas in the θ -direction, declined by the centrifugal force from the poles to the equator, decelerates to become zero at $\theta = \pi/2$. Behind these shocks a fast rotation region is observed (Figures 14 and 17). This region of highly rotating dense matter will form an accretion disk if $S < 1$.

6 DISCUSSION

Numerical simulation has been performed for axially symmetric rotating gas accretion on to a star. The second order space high-resolution Lax–Friedrichs-type scheme gave a good performance for the calculation of flows with very great variation of pressure and density values throughout the computational region. Flow

restructuring is investigated as the rotation velocity approaches the Keplerian velocity. The variants are presented for different cases starting from a slow rotation and up to the case for which the steady-state centrifugal and gravitational forces near the stellar equator are rather close. The values of angular momentum, however, were sufficiently small, so that at the inner boundary the centrifugal force was smaller than the gravitational force and the stationary accretion picture could be attained. If the angular momentum of the falling matter reaches the value for which the centrifugal force balances the gravitation at force before the matter falls on to the star (the inner boundary in our calculations) the matter stops near the equatorial plane and forms a disk. In the absence of viscosity the mass of the disk increases in time. In the presence of viscosity, which is especially efficient in the turbulent case, the matter in the disk loses its angular momentum and moves slowly towards the centre forming a stationary accretion disk (Lynden-Bell, 1969; Shakura, 1972). We are interested here in the problem of long-period pulsar formation for which the angular momentum is insufficient for accretion disk origin near the Alfvénic surface, where the dynamic pressure of the flow is balanced by the magnetic surface at the magnetosphere of the neutron star. To find the angular momentum of the matter falling on to the star during accretion from the stellar wind penetrating through the Alfvénic surface, we need to take into account the magnetic field. This work is now in progress.

Acknowledgement

This work was supported by the Russian Foundation of Fundamental Research under Grant No. 95-01-00835.

References

- Barmin, A. A. and Pogorelov, N. V. (1995) In *Proc. 1st Asian Conference on Computational Fluid Dynamics*, Hong Kong, January 16–19, 1995, The Hong Kong University of Science and Technology 1, 353–358.
- Barmin, A. A., Kulikovskij, A. G., and Pogorelov, N. V. (1996) *J. Comput. Phys.* **126**, 77.
- Beskin, V. S. and Pidoprygora, Yu. N. (1995) *Zh. Eks. Teor. Fiz.* **107**, 1025.
- Bisnovatyi-Kogan, G. S. (1989) *Physical Problems of the Theory of Stellar Evolution*, Moscow, Nauka (in Russian).
- Bisnovatyi-Kogan, G. S. (1991) *Astron. Astrophys.* **245**, 528.
- Illarionov, A. F. and Kompaneetz, D. A. (1990) *Mon. Not. R. Astron. Ser.* **247**, 219.
- Koide, H., Matsuda, T., and Shima, E. (1991) *Mon. Not. R. Astron. Ser.* **252**, 473.
- Lipunov, V. M. (1992) *Astrophysics of Neutron Stars*, Berlin, Springer Verlag.
- Lovelace, R. V. E., Romanova, M. M., and Bisnovatyi-Kogan, G. S. (1995) *Mon. Not. R. Astron. Ser.* **386**, 244.
- Lynden-Bell, D. (1969) *Nature* **223**, 690.
- Matsuda, T., Fujimoto, Y., Shima, S., and Sawada, K. (1989) *Prog. Theor. Phys.* **81**, 810.
- Nagase, F. (1989) *Publs. Astron. Soc. Jpn* **41**, 1.
- Ruffert, M. (1994) *Astrophys. J.* **427**, 342.
- Sawada, K., Shima, E., and Matsuda, T. (1989) *Mem. Fac. Eng. Kyoto Univ.* **51**, 124.
- Shakura, N. I. (1972) *Astron. Zh.* **49**, 921.
- Steinolfson, R. S., Pizzo, V. J., and Holzer, T. (1994) *Geophys. Res. Lett.* **21**, 245.